Ecological Engineering 63 (2014) 88–101

Contents lists available at ScienceDirect

Ecological Engineering

journal homepage: www.elsevier.com/locate/ecoleng

# Field and numerical assessment of turning pool hydraulics in a vertical slot fishway

Bryan A. Marriner[a], Abul Basar M. Baki[a], David Z. Zhu[a,*], Jason D. Thiem[b], Steven J. Cooke[b], Chris Katopodis[c]

[a] Department of Civil and Environmental Engineering, University of Alberta, Edmonton, Alberta T6G 2W2, Canada
[b] Fish Ecology and Conservation Physiology Laboratory, Department of Biology, Carleton University, 1125 Colonel By Drive, Ottawa, Ontario K1S 5B6, Canada
[c] Katopodis Ecohydraulics Ltd., 122 Valence Avenue, Winnipeg, Manitoba R3T 3W7, Canada

ARTICLE INFO

*Article history:*
Received 25 April 2013
Received in revised form 29 October 2013
Accepted 19 December 2013

*Keywords:*
Vertical slot fishway
Turning pool
Flow structure
Turbulence
Vortices
Computational fluid dynamics

ABSTRACT

Turning pools are common in fishways, they create a more compact design by enabling fishways to fold back on themselves. Despite this, little is known about the hydraulic characteristics of turning pools or how they are influenced by different design elements. This paper presents the results of a study on the hydraulics of turning pools in vertical slot fishways focusing on the Vianney-Legendre vertical slot fishway in Quebec, Canada, which is one of few fishways worldwide to successfully pass sturgeon (i.e., lake sturgeon, *Acipenser fulvescens*). Field velocity measurements taken in two pools and a computational fluid dynamics (CFD) model study were used to assess the turning pool hydraulics of seven design geometries. Parallel biological studies of sturgeon in the fishway revealed that turning pools were the location with the highest rate of failed passage, apparently associated with large vortices in the centre of the turning pools which serve to delay or inhibit passage. Interestingly, the velocity, and turbulence levels are comparable to results from regular pools in vertical slot fishways. The volumetric energy dissipation rate in turning pools is suitable for fish passage. Based on in silico modelling we revealed that the addition of a baffle wall extending from the inside centre wall of the pool reduced the size of the vortex and provided a resting area for ascending fish. Adding a baffle wall should be considered in turning pools with semi-circular or straight back walls. There is a need for research to evaluate exactly how fish respond to different turning pool designs but in the interim, the approach used here demonstrates the potential for using hydraulic studies to design turning pools in fishways that meet biological criteria and presumably increase passage efficiency.



## 1. Introduction

Fishways are constructed to help migratory fish overcome obstructions and restore river connectivity. Fishways function as a means of passage around hydraulic barriers for fish migrating both upstream and downstream (Clay, 1995; Katopodis and Williams, 2012). There is a diversity of fishway designs including engineered structures (e.g., pool and weir, Denil, and vertical slot) as well as nature-like fishways that look and function much like a natural stream (Clay, 1995; Katopodis et al., 2001; Baki et al., 2013). Canada alone has over 200 documented fishways (Hatry et al., 2013). Fishways have been subject to much study to understand their biological effectiveness and to identify opportunities for refining their design to improve passage (reviewed in Bunt et al., 2012; Katopodis and Williams, 2012; Noonan et al., 2012; Roscoe and Hinch, 2010; Williams et al., 2012). However, one aspect of fish passage that has received little study is the hydraulics and passage efficiency of turning pools.

Turning pools are often added when a fishway is built to pass over a relatively tall structure (Rajaratnam et al., 1997). The Seton River dam fishway in British Columbia, the Vianney-Legendre fishway in Quebec, and the Torrumbarry fishway in Australia are a few examples of vertical slot fishways with turning pools (Pon et al., 2009; Thiem et al., 2011; White et al., 2011). The primary functions of turning pools are to turn the flow, to minimize flow energy carry over between turning and regular pools, and to provide resting space for fish (Rajaratnam et al., 1997). Fishways with turning pools are more compact than equivalent fishways without turning pools as they economize on space and facilitate a more optimum location for the fishway entrance. Design guidelines recommend

* Corresponding author. Tel.: +1 780 492 5813; fax: +1 780 492 0249.
*E-mail address:* david.zhu@ualberta.ca (D.Z. Zhu).

0925-8574/$ – see front matter © 2013 Elsevier B.V. All rights reserved.
http://dx.doi.org/10.1016/j.ecoleng.2013.12.010

and field studies have confirmed that the entrance in a fishway be placed as close as possible to the hydraulic barrier, making it easier for fish to find (Bunt, 2001; Clay, 1995; Katopodis and Williams, 2012).

Several biological studies have identified potential problems with turning pools (e.g., Bunt et al., 2000; Thiem et al., 2011; White et al., 2011). In a companion study of fish migration, Thiem et al. (2011) studied the movements of 88 adult lake sturgeon *Acipenser fulvescens* as they attempted upstream passage at the Vianney-Legendre vertical slot fishway, hereinafter called the site fishway, in Quebec. Of 56 individuals that failed passage, 20 failed in the two turning pools out of a total of 17 pools; and fish spent disproportionately longer time in the turning pools than in the regular pools. Additionally, bony herring *Nematalosa erebi*, silver perch *Bidyanus bidyanus*, and golden perch *Macquaria ambigua* also appeared to have difficulty negotiating turning pools in a fishway in Australia (White et al., 2011). There are a number of potential explanations including confusion associated with complex flows, flow characteristics that exceed the swimming abilities of fish, or fish could actually be using such areas to rest. Although the delays may be associated with use of the turning pools to rest, the fact that a number of studies have found failures associated with turning pools is suggestive that there may be hydraulic challenges that impede passage. Unfortunately, there have been few attempts to characterize the hydraulic conditions within turning pools and relate flow characteristics to fish behaviour.

One of the more common types of fishway designs to incorporate turning pools is the vertical slot fishway. Its design functions over a range of upstream and downstream water levels, and allows fish to ascend at any depth in the water column (Liu et al., 2006; Rajaratnam et al., 1992). Vertical slot fishways are composed of regular pools connected in sequence forming linear ladders. Regular pools have been the subject of extensive study translating into a detailed understanding of their hydraulics, and the development of design standards (Liu et al., 2006; Puertas et al., 2004; Rajaratnam et al., 1992; Wu et al., 1999). In cases where the difference between upstream and downstream water levels is greater than the maximum allowable design slope, more than one segment of regular pools is required, leading to the use of one or more turning pools. Rajaratnam et al. (1997) completed a laboratory scale model study of a turning pool in a Denil fishway, but no hydraulic studies have been conducted for turning pools in vertical slot fishways.

Given the lack of existing hydraulic data accompanied by the comparatively low passage success rates there is cause for further study to evaluate and improve turning pool hydraulics, relative to fish passage. Here we characterize turning pool hydraulics of the Vianney-Legendre fishway using field based measurements and computational fluid dynamics (CFD) modelling. Annually, it passes over 35 species of fish (Thiem et al., 2013) and is one of few fishways worldwide to successfully pass a species of sturgeon, although delays and failures were noted for the species at turning pools (Thiem et al., 2011). In the case of the site fishway, three segments of regular pools are placed in series connected via two turning pools (see Fig. 1) creating a more compact design using a fold-back or staircase pattern, and thus making it a suitable model for a turning pool study. We first describe the site fishway, and present the methods used to obtain velocity results from measurements taken in the two turning pools. We then present a CFD model study which assesses seven turning pool design geometry alterations with respect to velocity, turbulent kinetic energy, vorticity, and flow structure. Design 1 simulates the site fishway's downstream turning pool, Designs 2–7 have design elements altered from Design 1. Field results are used to validate the CFD model study findings. Results are discussed in the context of what the turning pool hydraulic conditions may mean to fish behaviour. It is expected that the findings emanating from this study will help to supplement general fishway design guidelines and help to inform the design of turning basins that minimize delays and facilitate passage of fish.

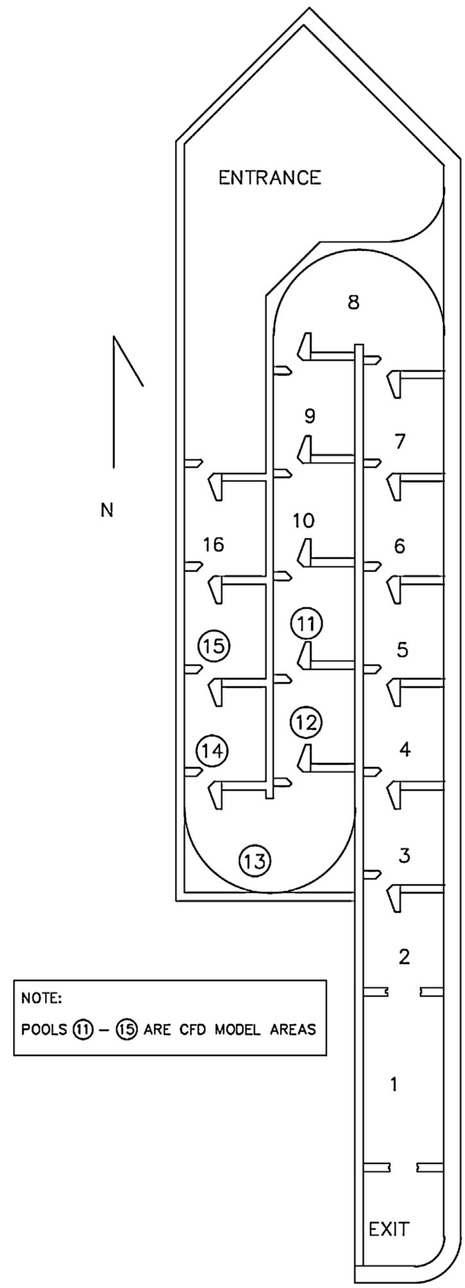


**Fig. 1.** Plan view diagram of the Vianney-Legendre vertical slot fishway, with pools labelled by number and circled numbers to identify the area simulated with computational fluid dynamics modelling.

## 2. Methods

### 2.1. Field study

The site fishway is on the Richelieu River in Quebec, a tributary of St. Lawrence River. It has 17 pools total; 13 regular pools, 2 turning pools, plus entrance and exit pools, see Fig. 1. It is formed of three linear ladders connected by two 180° turning pools, with fishway entrance and exit pools at the downstream and upstream ends of

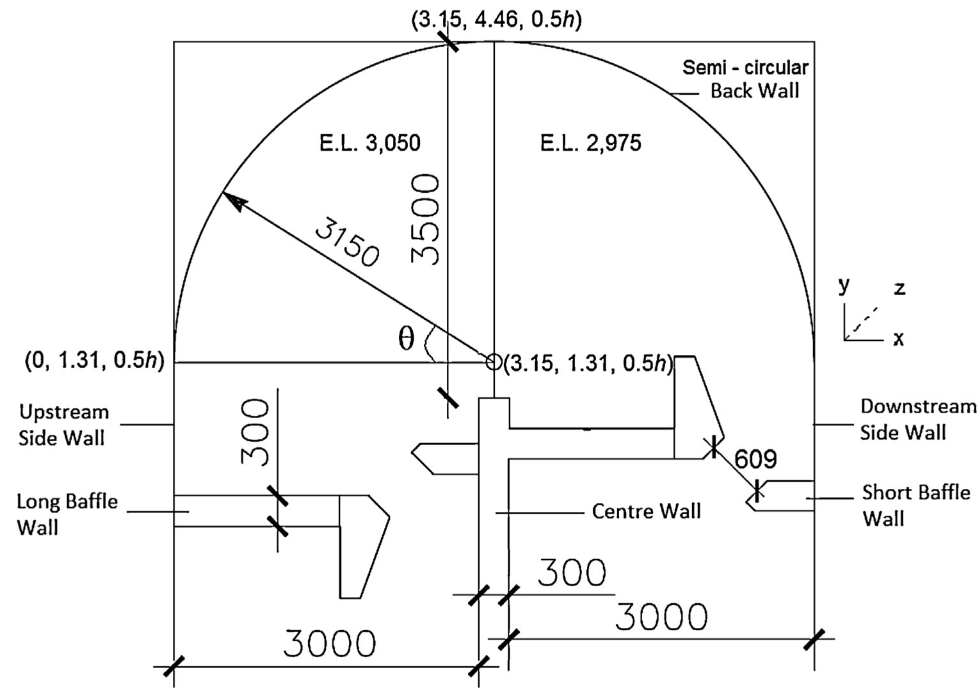


**Fig. 2.** Plan view schematic diagram of a turning pool, Pool 13 (Fig. 1), in the Vianney-Legendre vertical slot fishway; this geometry is simulated using CFD modelling in Design 1. Note: pool dimensions are presented in millimeters and point coordinates in meters.

the fishway. Water enters the upstream end of the fishway into Pool 1, flows through Pools 1–7 (ladder 1), turns 180° in Pool 8, flows through Pools 9–12 (ladder 2), turns 180° in Pool 13, flows through Pools 14–16 (ladder 3), and then exits into the river downstream of the dam. The length of the fishway, $L_F$, is 48.5 m and width, $B_F$, is 9.60 m. The elevation change within the fishway is 2.55 m, resulting in an overall fishway slope, $S_F$, of 2.8%, while the slope of ladders 1, 2, and 3 is 4%. The entrance pool is 12.50 m long, with a 3.50 m wide entrance gate. The exit pool is 15.63 m long and 3.0 m wide. Each turning pool has a width, $B_T$, of 6.3 m. The back wall is semi-circular with a radius, $R_T$, of 3.15 m. Pool 13, see Fig. 2, has a maximum length, $L_T$, of 3.50 m from centre wall to back wall, while Pool 8 is smaller with $L_T = 3.35$ m. Each turning pool floor is flat with a 7.5 cm elevation change at the pool's centre. Regular pools are 3.5 m long ($L_R$), and 3.0 m wide ($B_R$), the pool floor has a slope of 2.14% (7.5 cm elevation change) and the depth of water in the pool is $h$. There is a 7.5 cm elevation changes across the slot areas of Pools 2 – Entrance. The slot width, $b_0$, in all regular and turning pools is 0.609 m. The length and width to slot width ratios for turning and regular pools are $L_T = 5.5b_0$ and $5.75b_0$, $B_T = 10.34b_0$, $L_R = 5.75b_0$, and $B_R = 4.93b_0$. It is important to note that the ratios for regular pools at the site fishway are less than the recommended design ratios of $L_R = 10b_0$, and $B_R = 8b_0$ (Rajaratnam et al., 1992).

Fieldwork was conducted from July 18–29, 2011. Velocity point measurements were recorded in turning Pools 8 and 13 with a three-dimensional (3D) Acoustic Doppler Velocimeter (ADV). The ADV uses the Doppler shift to measure 3D point velocities (Nortek AS, 2009). Many recent fishway studies have used ADVs to measure 3D point velocities (e.g., Liu et al., 2006; Puertas et al., 2004, Silva et al., 2012). A grid spacing of 0.50 m × 0.50 m was used, with increased point densities in slot and jet flow areas. A total of 84 and 106 measurements were taken in Pools 8 and 13, respectively. The ADV field probe was submerged 0.50 m and fixed at that elevation for all points within the pool. The probe was mounted on a rigid frame constructed of modular t-slotted aluminium. The frame was mounted on pool walls to record measurements (Marriner, 2013).

Velocity measurements were recorded for 180 s at a sampling frequency of 25 Hz. Prior to data collection preliminary testing was done to determine the required ADV sampling period for accurate time-averaged velocity measurements. Sample test periods of 30–120 s were taken; velocity became nearly constant after 45 s. Longitudinal, transverse, and vertical velocities ($u$, $v$, and $w$), corresponding to $x$, $y$, and $z$ in the Cartesian coordinate system, were averaged over the sampling period to produce time-averaged velocities ($\bar{u}$, $\bar{v}$, and $\bar{w}$), see Fig. 2. The manufacturer specifies that the velocity data collected with the ADV is accurate to ±0.5% of the measured value, with a maximum accuracy of ±0.001 m/s (Nortek AS, 2009). The maximum velocity recorded was 1.4 m/s, with an accuracy of ±0.007 m/s. Velocity data for this study is expressed to 0.01 m/s. The ADV used in this study has a correlation scale of 0–100% (Nortek AS, 2009). The scale ranges from no correlation at 0% to perfect correlation at 100%. For time-averaged velocity magnitudes a minimum correlation of 40% is generally taken as acceptable. For all 190 of the ADV point measurements, the average correlation coefficient was 81%. Where the velocity magnitude was less than 0.6 m/s the average correlation was 84% and, where the velocity magnitude exceeded 0.6 m/s the average correlation was 56%. The lower correlation is attributed to vibrations of the ADV frame caused by the relatively large velocities. All measurements had a correlation above 40% and are accurate for time-averaged velocity calculations. A water level measuring data logger was used to record water levels in Pool 13 (Schlumberger Water Services, 2011). The data logger was placed on the downstream side of the centre wall, at the intersection with the long baffle wall. As the water surface in this fishway is three-dimensional, it was important to place divers in low velocity, and turbulence areas. This allowed the divers to suspend with little movement. Each measurement was recorded at a frequency of 1 min. Water level data is presented to 0.01 m, with an accuracy of ±0.01 m in this study. Water levels were recorded with a staff gauge on July 22, 2011 to assess the change in water level between adjacent pools, $\Delta h$. Measurements were taken at $x = 1.50$ m (the centre of the attached regular pool) on both sides of the long baffle wall at the upstream end of turning pools, see Fig. 2. Each measurement was recorded and averaged over 1 min and is accurate to ±0.01 m (Marriner, 2013).

### 2.2. CFD modelling

#### 2.2.1. Governing equations

A commercial software programme was used to create a numerical model simulating Pools 11–15, see Fig. 1 (ANSYS, 2009). The model uses the finite volume method to solve the Reynolds averaged Navier–Stokes equation in three-dimensions. It models the *free surface*, the interface between air and water, following the volume of fluid (VOF) method. The VOF method solves a set of momentum equations through the domain, while maintaining a record of the volume of the two phases in each computational cell. The software programme solves the continuity and momentum equations (in tensor form) as follows:

$$\frac{\partial \rho}{\partial t} + \frac{\partial \rho u_j}{\partial x_j} = 0$$
$$\frac{\partial \rho u_i}{\partial t} + \frac{\partial \rho u_j u_i}{\partial x_j} = -\frac{\partial p}{\partial x_i} + \frac{\partial}{\partial x_j}\left\{(\mu+\mu_t)\left(\frac{\partial u_i}{\partial x_j} + \frac{\partial u_j}{\partial x_i}\right) - \frac{2}{3}\rho k \delta_{ij}\right\} + (\rho - \rho_a) g_i \quad (1)$$

where $\delta_{ij}$ is the Kronecker delta, $g$ is the gravitational force, $k$ is the turbulent kinetic energy, $\mu$ is the molecular viscosity of fluid, $\mu_t$ is the turbulent viscosity of fluid, $p$ is the static pressure, $\rho$ is the fluid density, and $\rho_a$ is the density of air. The standard $k-\varepsilon$ model, where $\varepsilon$ is the turbulent kinetic energy dissipation rate, was used to determine the turbulent viscosity (Launder and Spalding, 1974). Previously, Khan (2006) used this model for a vertical slot fishway and Kirkgoz et al. (2009) showed this model performed better than the $k-\omega$ model for predicting the velocity field over a chute spillway.

Eq. (1) uses the volume fraction of air and water phases in the physical properties of density and viscosity. The phase-averaged density and viscosity are as follows:

$$\rho = \alpha_w \rho_w + \alpha_a \rho_a \quad (2)$$

$$\mu = \alpha_w \mu_w + \alpha_a \mu_a \quad (3)$$

where $\alpha$ is the volume fraction, with subscripts $a$ and $w$ representing the air and water phases. When modelling the free surface the transport equation is used to represent the water phase and is defined by:

$$\frac{\partial \alpha_w}{\partial t} + u_j \frac{\partial \alpha_w}{\partial x_j} = 0 \quad (4)$$

In this case the air phase volume fraction is determined from the constraint and the transport equation is simplified to:

$$\alpha_a = 1 - \alpha_w \quad (5)$$

Eq. (5) is solved across the entire domain and the volume fraction is computed for all cells within the domain. In the main flow region cells are filled with water and $\alpha_w = 1$. In cells filled with air $\alpha_w = 0$. Interface tracking occurs in cells where $0 < \alpha_w < 1$. These cells contain a combination of air and water and are located on the *free surface*.

In a homogeneous model the mass transfer terms between phases are neglected (Fernandes et al., 2008,2009). Comparatively, the VOF model takes into account the surface tension along the phases interface. The simulations ran in this experiment use the surface tension model continuum surface force (CSF) (Brackbill et al., 1992). CSF models the surface tension force as a volume force concentrated at the interface, as opposed to a surface force.

#### 2.2.2. Boundary conditions and computational mesh

The model's pool geometries match the dimensions of the field fishway. Boundary conditions are applied to all faces of the domain (pool walls and floor). The mass flow rate was specified at the upstream inlet boundary and atmospheric pressure was applied at the downstream boundary of the domain. At the upstream boundary the turbulence intensity ($I$) was set to 10% to take into account the effect of strong turbulence and recirculation in the flow field. However, it has been shown that the predicted velocities are graphically indistinguishable for 5%, 10%, and 20% turbulence intensities (Ma et al., 2002).

Given a known intensity the software programme uses the following expressions to compute $k$ and $\varepsilon$ at the boundary inlet (ANSYS, 2009):

$$k_{in} = \frac{3}{2} I^2 u_{in}^2 \quad (6)$$

And

$$\varepsilon_{in} = \rho C_\mu \frac{k^2}{100 I \mu_t} \quad (7)$$

For the $k-\varepsilon$ turbulence model $C_\mu$ is the constant and has a value of 0.09. The top surface is an open boundary and is a pressure boundary allowing both inflow and outflow. The no-slip condition and roughness heights of 2 mm were applied to all of the model's surfaces. While not directly measured in the field, the likely representative range of roughness height for the site fishway's 12-year-old concrete wall will be 1–3 mm. The simulated results for roughness heights 0.14 mm and 2 mm in this study revealed that the effect of the roughness height is limited to within 0.1 m to the wall. This is in agreement with previous practical experiences that have demonstrated that roughness height is not the dominant factor in determining the overall circulation pattern in a hydraulic structure (Khan et al., 2005).

The model was simulated for two different scenarios. In the first scenario $\Delta h$ between Pools 12 and 13 was set equal to 0.09 m, as measured in the field; and the maximum slot velocity vector, $V_{sm}$, measured in the field is equivalent to the CFD simulated value. The first is used for the purpose of comparing CFD simulated data to the field measured values in Pool 13. The second scenario has a larger $\Delta h$ (0.11 m) and a 15% higher volumetric flow rate. This scenario produced larger velocities and represents spring conditions. Spring conditions were chosen because the site fishway is most frequently used in the spring months (Thiem et al., 2011). All results and discussion in this paper focus on the values simulated in the second scenario. In both scenarios at the inlet boundary an initial longitudinal velocity was fixed while transverse and vertical velocities were set to zero. At the outlet boundary, the initial pressure was assumed to be hydrostatic in the water region and zero in the air region. In addition to the velocity and hydrostatic pressure water levels were fixed at the inlet and outlet to specify the water volume fraction at the boundary.

The model uses an upwind scheme for advection. It also uses an unstructured tetrahedral mesh in the solution domain. The model convergence criterion is 0.0001. The numerical iteration is continued until the non-dimensional residual of each of the velocity, turbulent kinetic energy and dissipation, and mass is less than

**Table 1**
Summary of mesh properties as tested to assess the effect of mesh size on numerical modelling results.

| Mesh number | 1 | 2 | 3 |
|---|---|---|---|
| Size (m) | 0.14 | 0.12 | 0.11 |
| Nodes | 171,399 | 271,974 | 352,082 |
| Elements | 927,754 | 1,485,274 | 1,932,418 |

0.0001. All simulations were run under steady state conditions and the model converged after less than 600 iterations.

To determine the result's sensitivity to simulation grid size a mesh independency study was conducted using the simulation of Pool 13 (Design 1). Three mesh sizes were tested to assess the effect of mesh size on numerical results. The meshes are summarized in Table 1. Two points were selected to test the mesh independency. The first point was at (4.04, 2.86) and the second at (1.54, 1.86). The combined average velocity difference for both points is 0.014, 0.0 21 and 0.031 m/s when comparing mesh 1–2, mesh 2–3, and mesh 1–3, respectively. Fig. 3 shows the results of the mesh independency test. After the test was completed all simulations were run with mesh 3.

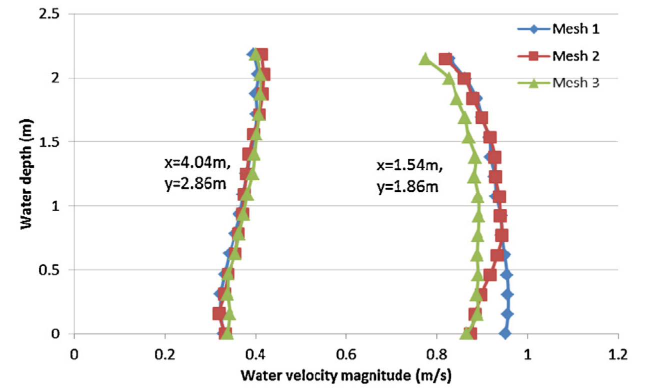


**Fig. 3.** Results of the mesh independency test completed to determine the sensitivity of grid size on numerical results of Design 1.

### 2.3. Design modifications and evaluation criteria

CFD modelling was used to simulate the hydraulics of the existing conditions in Pool 13 (Design 1), see Fig. 2. Six additional designs were simulated, Designs 2–7 (see Fig. 4), each having geometric elements differing from Design 1. Plan view schematic diagrams of these six designs, Designs 2–7 are shown in Fig. 4 (a)–(f). A baffle wall is added to the pool's centre in Designs 2, 3, and 4. It is 0.30 m × 1.50 m in Designs 2 and 3, and 0.3 m × 2.0 m in Design 4. The purpose of adding a baffle wall is to reduce the size of the vortex in the pool's centre in Design 1 (see Section 3) and to provide fish with resting space in the turning pools. The position is altered in these three designs to assess the influence position has on hydraulics. Alterations to the pool floor are made in Designs 5 and 6. In Design 5 the floor is sloping at 3.5%, a 0.225 m elevation drop from the upstream side wall to the downstream side wall. This is the maximum slope allowable given the restrictions of the connecting pools (Pools 12 and 14). The pool floor ramps from the outer wall radially inward about the end of the centre wall at 10% in Design 6. These geometry alterations to the pool floor were tested to encourage flow in the downstream direction, and to reduce flow recirculation. Design 7 has a straight back wall, different from the semi-circular back wall in Designs 1–6. The straight back wall is less expensive to construct than a semi-circular back wall, and has been constructed at several vertical slot fishways, e.g., Seton River dam fishway, British Columbia (Pon et al., 2009). However, it should

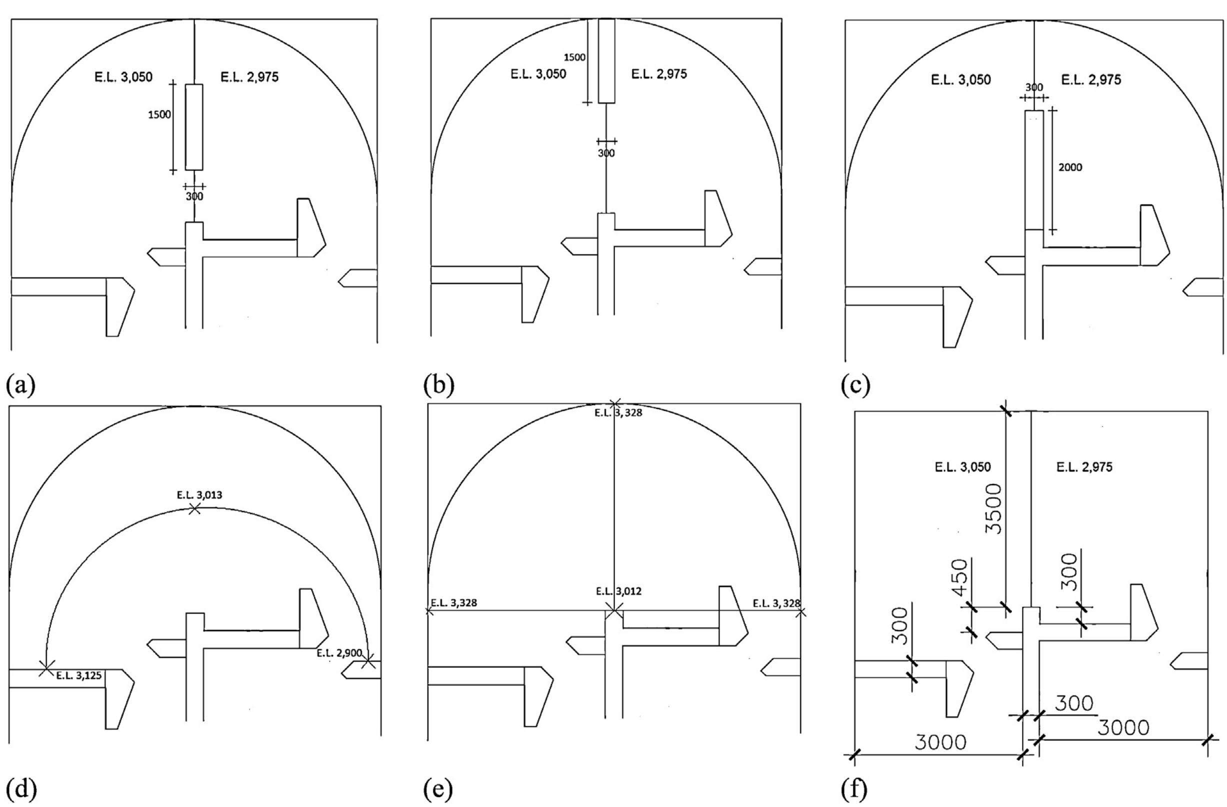


**Fig. 4.** Plan view schematic diagrams of vertical slot turning pool designs: (a) Design 2, (b) Design 3, (c) Design 4, (d) Design 5, (e) Design 6, and (f) Design 7.

be mentioned that in a few cases, the dam owners and resource agency personnel initially chose this less expensive Design 7, but then decided to round corners using wooden walls, e.g., Brunswick dam on the Androscoggin River in State of Maine (Brown et al., 2010). Further study might be needed to identify the suitability of this design.

Designs simulated in this study are evaluated on velocity, and two turbulence parameters, turbulent kinetic energy and vorticity. Velocity is typically the major consideration in fishways. To allow fish to ascend through the pool the maximum flow velocity must be less than the maximum attainable swimming speed. Typically, burst or prolonged modes are considered, a positive ground speed is required for successful passage (swimming speed must be greater than water velocity), and the combination of distance and velocity should not exceed endurance (Peake et al., 1997). Turbulent kinetic energy represents one turbulence parameter that could potentially affect fish passage through a fishway. Fish typically expend more energy swimming in comparatively high turbulent flows than in low turbulent flows (Enders et al., 2003, 2005), and have significantly lower swimming capabilities in turbulent flows as compared to laminar flows (Pavlov et al., 2000). In fishways, preferences to areas with 'low' turbulent kinetic energy levels over areas of 'high' turbulent kinetic energy levels have been demonstrated, and a negative correlation exists between fish transit time (the length of time a fish requires to successfully ascend a fishway pool) and turbulent kinetic energy levels (Silva et al., 2012). Vorticity was used in design evaluation as recent studies assessing the effects of vortex size on the swimming capabilities of fish have found that when the diameter of a flow vortex oriented in the horizontal plane, $D_V$, exceeded 0.5–0.75 of fish body length, $l_f$, fishes swimming capabilities were challenged. Fish spun in an orientation consistent with the rotational axis of the vortices and translated downstream. To combat the loss of balance fish used their pectoral fins to restore spatial balance control, forcing them to expend more energy to maintain spatial balance control and leaving less energy to swimming speeds (Lupandin, 2005; Tritico and Cotel, 2010; Webb and Cotel, 2010). The flow patterns in turning pools in which the streamlines are concentric circles are highlighted by a large recirculation area, or recirculation eddies. Within the circulation eddy, the fluid particles rotate as they revolve around the vortex centre. Due to the asymmetric geometry the jet does not enter through the pool's centre and there are two flow recirculation eddies sitting on either side of the jet. This study measures the length and width dimensions of the circulation eddy in the centre of the pool as its velocity vectors wraps into itself. The length and width dimensions are evaluated because the circulation eddies in the turning pool are not circular because of the pool's geometry.

Time-averaged velocity magnitude, $V$, is defined as:

$$V = \sqrt{\bar{u}^2 + \bar{v}^2 + \bar{w}^2} \tag{8}$$

where $\bar{u}$, $\bar{v}$, and $\bar{w}$ represent the longitudinal ($x$), transverse ($y$), and vertical ($z$) components of time-averaged velocity, respectively. Turbulent kinetic energy, $K$, is defined as:

$$K = \frac{1}{2}(u'^2_{rms} + v'^2_{rms} + w'^2_{rms}) \tag{9}$$

where $u'$, $v'$ and $w'$ are the longitudinal, transverse, and vertical fluctuating velocities, respectively. $K$ levels are categorized as 'low' for $K \le 0.05\,\mathrm{m^2/s^2}$ and 'high' for $K > 0.05\,\mathrm{m^2/s^2}$ (Silva et al., 2012). Vorticity in the horizontal ($x$, $y$) plane, $\omega_Z$, is the magnitude of rotation about the $z$-axis and is defined as:

$$\omega_z = \frac{1}{2}\left(\frac{\partial\bar{u}}{\partial y} - \frac{\partial\bar{v}}{\partial x}\right) \tag{10}$$

where $\partial\bar{u}/\partial y$ and $\partial\bar{v}/\partial x$ are components of angular velocity in along the x-axis and y-axis, respectively. The vorticity calculated is time-averaged, assuming that the flow field is time averaged (Jamieson et al., 2013). $\omega_Z$ levels are categorized as 'low' for $\omega_Z \le 3.0\,\mathrm{s^{-1}}$ and 'high' for $\omega_Z > 3.0\,\mathrm{s^{-1}}$.

The average volumetric energy dissipation, $\bar{\delta}$, in the turning pool is defined as:

$$\bar{\delta} = \frac{\rho g Q \Delta h}{B_T L_T y_0} \tag{11}$$

where $Q$ represents the volumetric flow rate, and $y_0$ represents the depth of flow. In Eq. (11), the numerator represents the energy dissipation and the denominator is the volume of a rectangular turning pool. In cases where the pool is not rectangular, such as Pool 8, Pool 13 and Designs 1–6 which have semi-circular back walls, the denominator in Equation 11 is adjusted to represent each design's volume. $\bar{\varepsilon} = 29\ \ \mathrm{W/m^3}$ in Pool 13 where $\Delta h = 0.09\,\mathrm{m}$, $y_0 = 2.34\,\mathrm{m}$, and $Q = 1.63\,\mathrm{m^3/s}$. $\bar{\varepsilon}$ is less than the calculated range, $\bar{\varepsilon} = 92\text{–}180\ \ \mathrm{W/m^3}$ for a regular pool (Liu et al., 2006).

## 3. Results

### 3.1. Field results and CFD model validation

The maximum slot velocity vector, $V_{sm}$, is 1.40 m/s in Pools 8 and 1.15 m/s in Pool 13. During the 2011 field study high water levels downstream of the site dam effected pool water levels. As measured in the field on July 22, 2012 the high downstream water levels caused $\Delta h$ to decrease towards the downstream end of the fishway, $\Delta h = 0.17$ m between Pools 7 and 8, and $\Delta h = 0.09$ m between Pools 12 and 13. As expressed in Equation 12 below, the comparatively greater $\Delta h$ between Pools 7 and 8 produced a greater $V_{sm}$ magnitude. The theoretical maximum slot velocity, $V_{theor}$:

$$V_{theor} = \sqrt{2g\Delta h} \tag{12}$$

is derived from the Bernouli equation. Assuming velocities in the pools are negligible, water elevation difference between adjacent pools produces a maximum velocity magnitude in the slot area of $V_{theor}$. In Pool 13, $V_{sm}$ and $\Delta h$ were measured concurrently and Equation 12 was used to calculate $V_{theor} = 1.33$ m/s. $V_{theor}$ is 16% greater than $V_{sm}$. Therefore, $V_{theor}$ can be used to reliably estimate $V_{sm}$ in turning pools. This agrees with results from regular pool research where $V_{theor}$ is approximately equal to $V_{sm}$ (Liu et al., 2006). It is important to note that in Pool 8, the measurement of $V_{sm}$ and $\Delta h$ were not concurrent: $\Delta h$ and $V_{sm}$ were measured on 22nd and 27th of July, respectively. Therefore, $V_{\mathrm{sm}}$ to $V_{\mathrm{theor}}$ comparison is not applicable for Pool 8.

The mean time-averaged vertical velocity, $\bar{w}_{ave}$, is defined as the average of vertical velocities measured with the ADV in the field for each respective pool. It is −0.01 m/s in both Pools 8 and 13. The maximum vertical velocity, $\bar{w}_{\max}$, is 0.15 m/s and 0.14 m/s in Pools 8 and 13, respectively, which is less than 0.1 $V_{sm}$ in both pools. The comparatively low vertical velocities show turning pool flows are primarily in the $x$, $y$ plane as is characteristic in regular pools (Liu et al., 2006; Puertas et al., 2004).

The velocity field diagram for Pool 13 is shown in Fig. 5. It presents the resultants of the $\bar{u}$, $\bar{v}$ velocity vectors in the $x$, $y$ plane at an elevation of 1.74 m above the pool floor (approximately 0.50 m below the water surface). Pools 8 and 13 have a common flow pattern. Flow enters the pool through the upstream slot as a jet, flows with high velocity towards the back wall, turns flowing along the semi-circular back wall, and flows out through the downstream slot. A 3.0 m long, $L_V$, and 2.1 m wide, $B_V$, recirculation area, or vortex, forms in the centre of the pool. A second, smaller recirculation area is located in the upstream corner of the pool between the

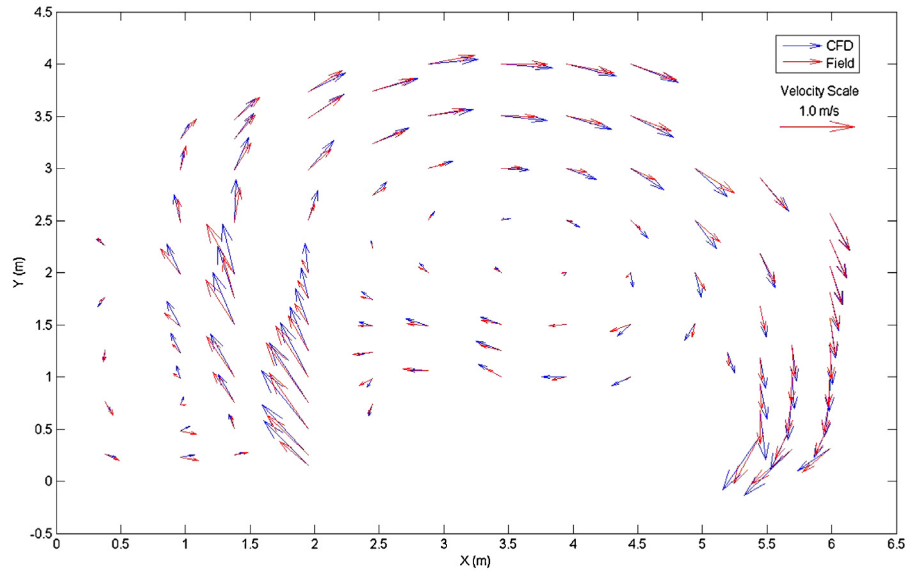


**Fig. 5.** Velocity data points comparison between field measurements taken in Pool 13 of the Vianney-Legendre vertical slot fishway and results simulated in Design 1 with CFD modelling.

long baffle and side walls. These two areas are characterized by low velocities and recirculating flow.

For scenario one the flow pattern simulated in Design 1 is consistent with the field pattern measured in Pool 13, see Fig. 5. In both Pool 13 and Design 1 the vortex in the centre of the pool is equal in length and width, see Table 2. Fig. 5 compares the field velocity data measured in Pool 13 to the CFD simulated velocities of Design 1 at an elevation of 1.74 m above the pool floor. All 106 field measurements were used for comparison. The mean absolute error (MAE), MAE = |CFD predicted velocity − measured mean velocity|, was 0.06 m/s. The value of $\Delta h$ between Pools 12 and 13 is equal to 0.09 m and $V_{sm}$ is equal to 1.15 m/s for both field measurements

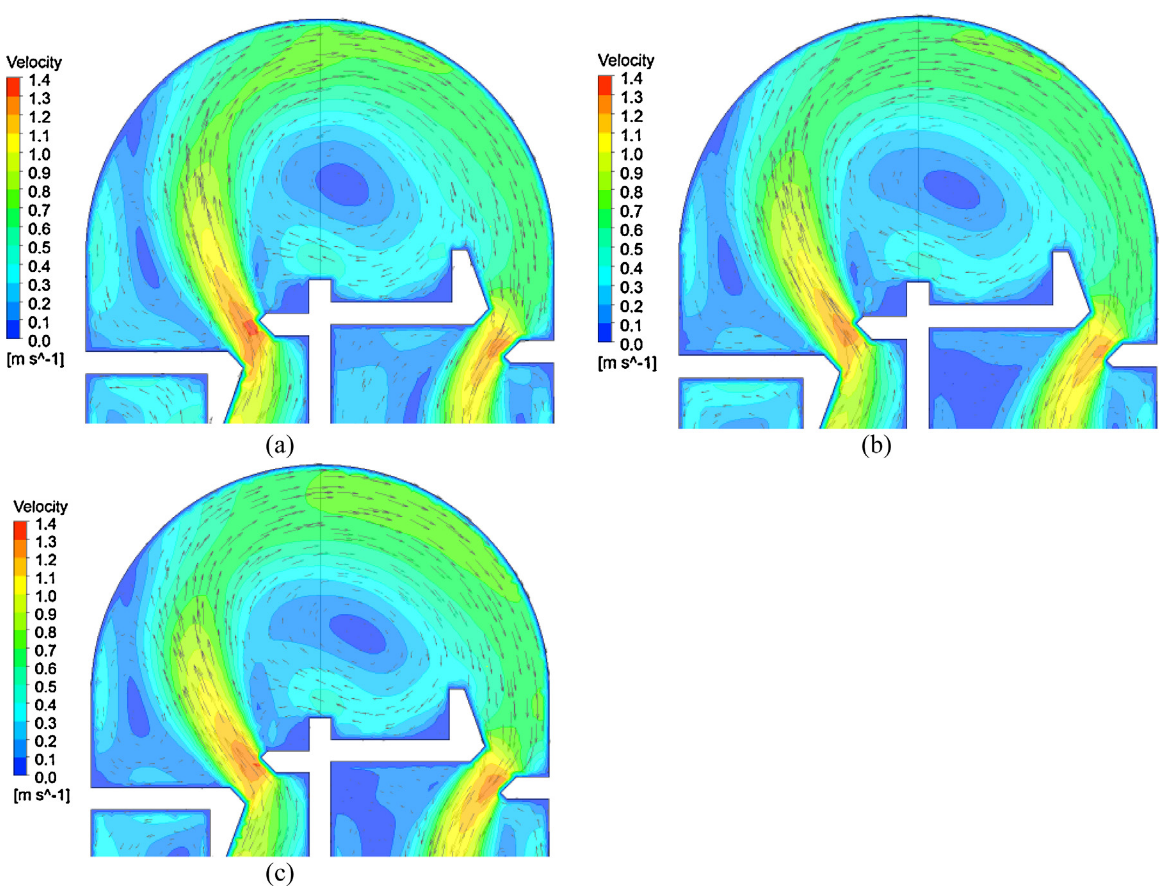


**Fig. 6.** Velocity magnitudes and directions in turning pool Design 1: (a) at depth $z = 0.13h$, (b) at depth $z = 0.5h$, (c) at depth $z = 0.8h$.

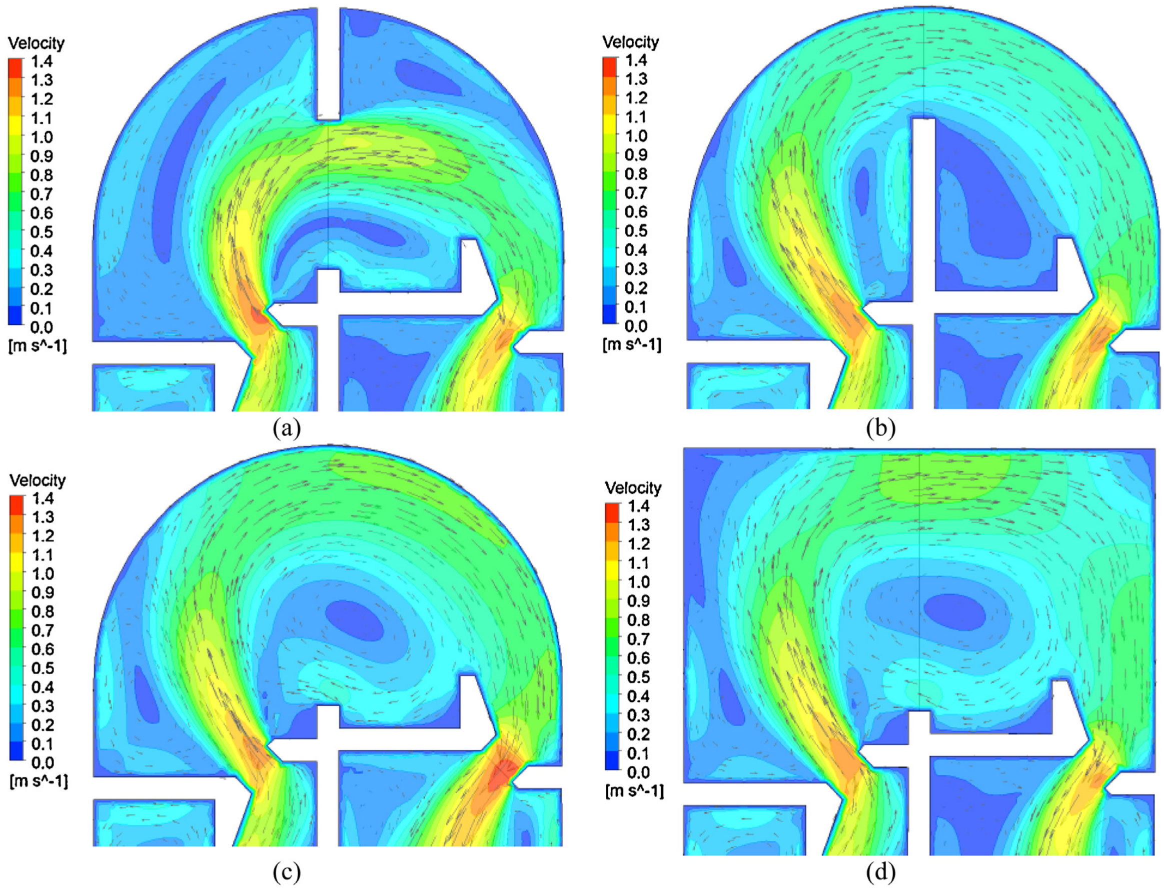


**Fig. 7.** Velocity magnitudes and directions at depth $z = 0.5h$ in turning pool designs: (a) Design 3, (b) Design 4, (c) Design 6, and (d) Design 7.

and CFD simulated results. This demonstrates agreement between field measured and CFD simulated velocity data.

### 3.2. CFD model results

Velocity, turbulent kinetic energy, and vorticity results are presented for Designs 1, 3, 4, 6, and 7. Adding a 1.5 m × 0.3 m baffle wall to the centre of the pool, perpendicular to the back wall, in Design 2 did not significantly vary from the hydraulics from Design 1; nor did a 3.5% slope of the pool floor, in Design 5. Consequently, the hydraulics of Designs 2 and 5 have been omitted. Results were simulated for depths of $z = 0.13h$, $0.5h$, and $0.8h$; where $z$ is measured from the pool floor upwards. These three depths represent the full height of the water column (Silva et al., 2011). Note that $0.13h$ is 0.30 m above the pool floor in this study's set of simulations and represents the hydraulics a fish swimming along the bottom of the pool would encounter and was selected because sturgeon are typically considered a benthic species.

**Table 2**
Summary of turning pool vortex lengths and widths for Pools 8 and 13, and Designs 1, 3 4, 6, and 7.

| Design | $L_V$ (m) $x$-dir. | $B_V$ (m) $y$-dir. |
|---|---|---|
| Pools 8 and 13 | 3.0 | 2.1 |
| 1 | 3.0 | 2.1 |
| 3 (centre) | 1.9 | 1.2 |
| 3 (upstream) | 1.3 | 4.5 |
| 3 (downstream) | 1.8 | 1.3 |
| 4 (upstream) | 0.9 | 2.0 |
| 4 (downstream) | 1.4 | 2 |
| 6 | 3.0 | 2.1 |
| 7 | 3.2 | 2.5 |

As shown in Figs. 6 and 7, the slot entrance holds the maximum flow velocity for all designs. $V_{sm}$ ranged from 1.3 to 1.4 m/s in the 7 designs tested. $V_{sm}$ is consistent through the full height of the water column for all designs. This is demonstrated in Fig. 6 for Design 1, where $V_{sm}$ = 1.35–1.4 m/s at $z = 0.13h$, $0.5h$, and $0.8h$.

The flow pattern in Design 1 is consistent with the pattern in Pool 13. The vortex in the centre of the pool is 3.0 m × 2.1 m. Vortex dimensions are summarized in Table 2 and flow patterns for all designs are shown in Figs. 6 and 7. The flow pattern and vortex dimensions in Design 6 are consistent with Design 1. However, the ramping floor accelerates flow around the back wall producing comparatively larger velocities through the downstream section of the pool. The straight back wall gives Design 7 a comparatively larger pool volume, correspondingly the vortex (3.2 m × 2.5 m) in the centre of the pool is larger than in other designs. A low velocity zone forms in the upstream back corner of the pool in Design 7. The baffle wall added to Designs 3 and 4 alters size and shape of the large recirculation area. In Design 3 jet flow is forced through the centre of the pool, inside of the centre baffle wall. A large recirculation zone (1.9 m × 2.0 m) forms between the jet flow and centre wall. Recirculation areas also form upstream (1.3 m × 4.5 m) and downstream (1.8 m × 1.3 m) of the centre baffle wall. In Design 4 the centre baffle wall forces high velocity flow around the back wall, and smaller recirculation zones form on both sides of the centre baffle wall. The upstream vortex is 0.9 m × 2.0 m, and the downstream vortex is 1.4 m × 2.0 m.

The variation of maximum velocity, $V_m$, as it flows through the pool from entrance to exit is shown in Fig. 8, where $x_m$ is

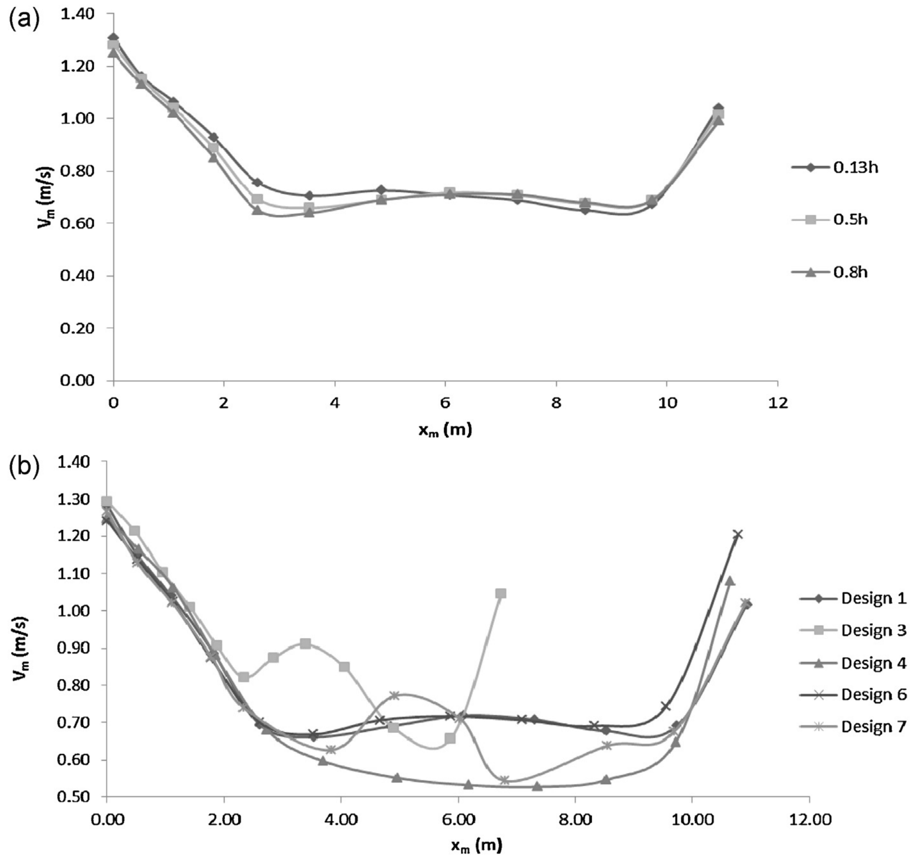


**Fig. 8.** Variation of maximum velocity, $V_m$, through the turning pool; where $x_m$ is the path of $V_m$ from the slot entrance to the slot exit: (a) Design 1 at depths of $z = 0.13h$, $z = 0.5h$, and $z = 0.8h$; (b) Designs 3, 4, 6, and 7 at depth of $z = 0.5h$.

the distance from the entrance slot along the flow path of $V_m$. As demonstrated by Design 1 in Fig. 8a the patterns of $V_m$ are nearly uniform at $z = 0.13h$, $0.5h$, and $0.8h$; this is also characteristic of the other designs tested. In Designs 1, 4, 6, and 7 $V_m$ decays rapidly over $x_m < 2.5$ m. At $x_m \cong 2.5$ m decay stops after reaching minimum magnitudes of 0.4–0.6 $V_{sm}$. Through the middle of the pool, $2.50\text{ m} < x_m \leq 9.0$ m, $V_m$ is nearly constant. In this section Design 4 maintains the lowest velocities, $V_m = 0.53$–$0.55$ m/s, while $V_m$ in Designs 1, 6, and 7 are 0.1–0.2 m/s greater. In the downstream section ($x_m > 9.0$ m), velocities increase linearly, reaching maximums in the downstream slot. The flow path length is approximately 11 m in these designs. The centre baffle wall position in Design 3 forces $V_m$ through the centre of the pool. As a result $V_m$ in Design 3 follows a flow path approximately 4.0 m

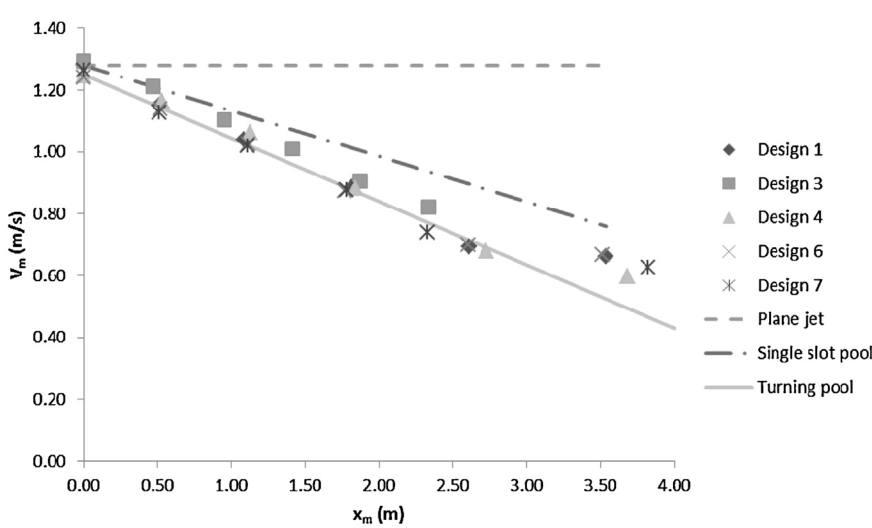


**Fig. 9.** Maximum velocity, $V_m$, decay comparison of a single slot pool, a plane jet, and turning pool Designs 1, 3, 4, 6, and 7 at a depth of $z = 0.5h$.

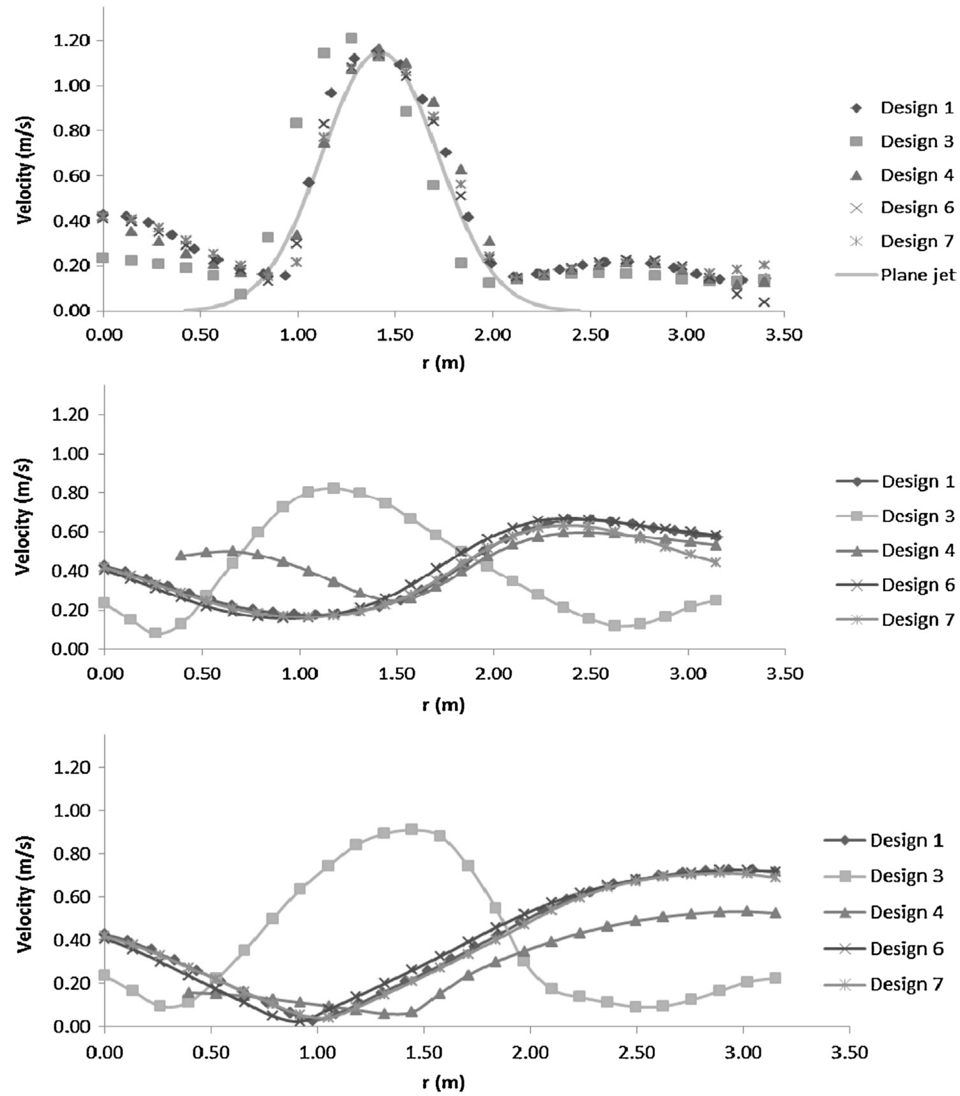


**Fig. 10.** Radial velocity distributions of Designs 1, 3, 4, 6, and 7 at $z = 0.5h$: (a) $\theta = -27°$, (b) $\theta = 67.5°$, (c) $\theta = 112.5°$.

shorter than in other designs and has comparatively greater $V_m$ magnitudes through the pool.

The rate of $V_m$ decay is compared to that of a plane turbulent jet, and to a regular pool in Fig. 9. In the designs simulated, for $x_m < 2.5$ m, $V_m$ decays at a linear rate described as:

$$\frac{V_m}{V_{sm}} = 1 - 0.05\frac{x_m}{0.5b_0}. \tag{14}$$

The decay of a plane turbulent jet is described as (Rajaratnam, 1976):

$$\frac{V_m}{V_{sm}} = \frac{3.5}{\sqrt{x_m/0.5b_0}} \tag{15}$$

The decay of a regular pool is described as (Liu et al., 2006):

$$\frac{V_m}{V_{sm}} = 1 - 0.035\frac{x_m}{0.5b_0}. \tag{16}$$

The decay of $V_m$ in the turning pool does not correlate to the decay in a turbulent plane jet. This is because the potential core of a turbulent plane jet is $6b_0$; at $x_m = 6b_0$ velocity in the turning pool is no longer in decay. Therefore, before a turbulent plane jet begins to decay, turning pool decay is complete. As expressed in Eqs. (14) and (16) the velocity decays faster in the turning pool as compared to a regular pool. The more rapid decay is thought to be caused by the 180° turn required in the pool. The controlling factor for velocity decay stopping and reaching a minimum $V_m$ at $x_m \cong 2.5$ m is the distance from the slot entrance to the back wall. In the designs simulated this distance is 4.46 m measured in the $y$-direction. As shown in Figs. 6 and 7, $V_m$ decays from the slot entrance until $x$, $y = (2.5$ m, $3.22$ m$)$, approximately 1.24 m from the back wall. At this point $V_m$ becomes constant as it turns and flows along the back wall. Similar to a regular pool, the rapid decay in the turning pool is thought to be caused by the recirculating flows that surround the jet (Liu et al., 2006).

Velocity distributions were taken perpendicular to the jet trajectory to understand the structure of flow in different sections of the pool. Distributions were taken from the centre of the pool, at $(x, y, z) = (3.15, 1.31, 0.5h)$, to the outer wall at angles, $\theta$, see Fig. 2, of $-44°$, $-27°$, $0°$, $22.5°$, $45°$, $67.5°$, $90°$, $112.5°$, $135°$, $157.5°$, $180°$, and $200°$. The line of $\theta = 0°$ is from $(0, 1.31, 0.5h)$ to $(3.15, 1.31, 0.5h)$, is parallel to the baffle walls, $\theta$ increases in the clockwise direction, and $V_m$ is the maximum velocity. The velocity distributions at $\theta = -22°$, $67.5°$, and $157.5°$ are presented in Fig. 10, where $r$ is the radial distance from $(3.15, 1.31, 0.5h)$ in the direction of $\theta$.

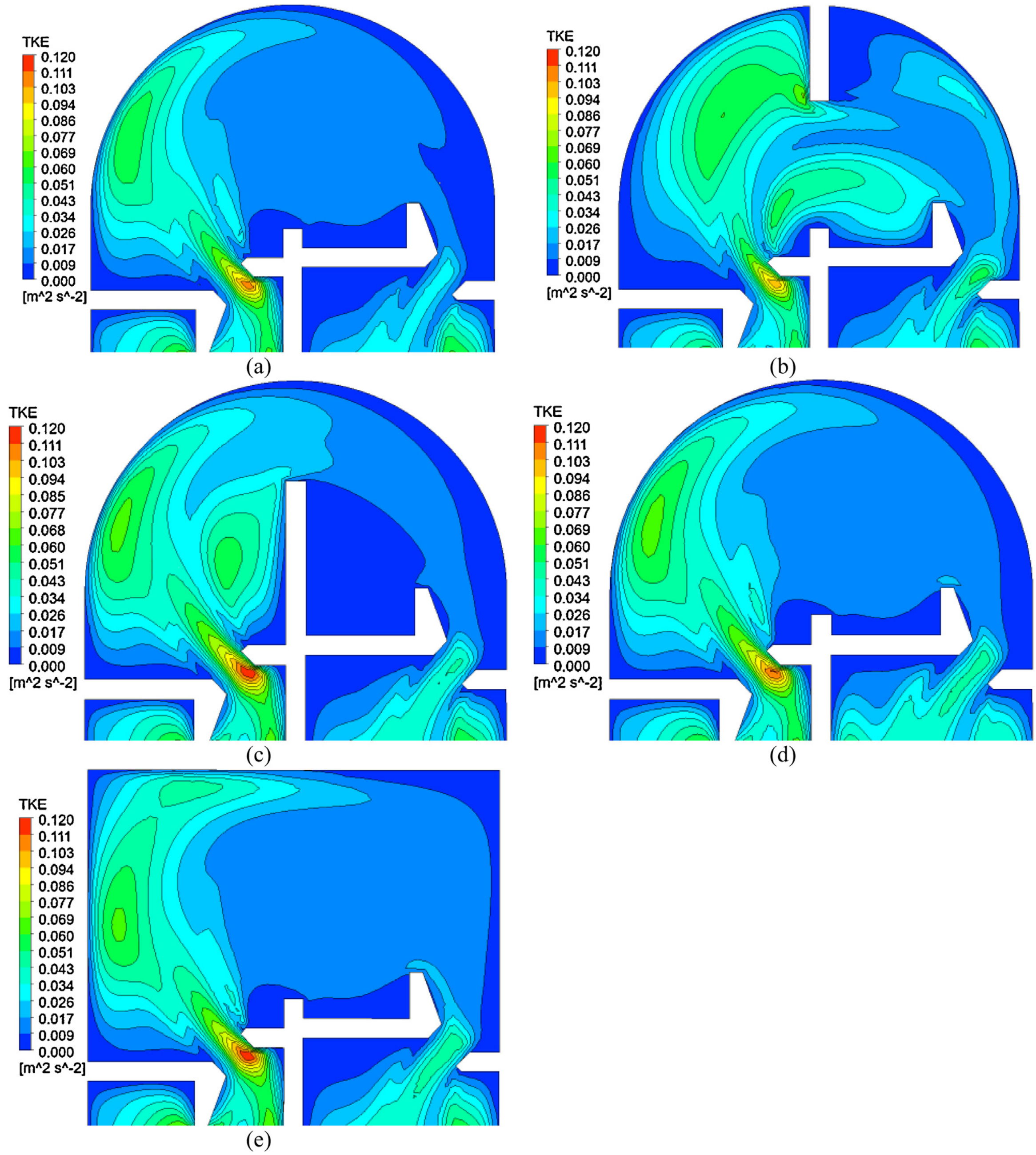


**Fig. 11.** Turbulent kinetic energy levels at depth $z = 0.5h$ in turning pool designs: (a) Design 1, (b) Design 3, (c) Design 4, (d) Design 6, and (e) Design 7.

At $\theta = -27^\circ$, upon entering the pool through the upstream slot the velocity distribution is of Gaussian distribution similar to a plane turbulent jet, see Fig. 10a (Rajaratnam, 1976). The velocity profile is approximately a turbulent plane jet for $-0.95b_0 < x_r < 0.95b_0$, where $x_r$ is the radial distance from $V_m$. The scatter outside is caused by recirculating flows on either side of the jet. In this profile $V_m$ ranges from 1.13 to 1.15 m/s at $r = 1.27$–1.42 m; the jet width at $V = ½V_m$, is 0.70 m = $1.15b_0$. In Designs 1, 4, 6, and 7 the velocity profile changes from a Gaussian distribution as θ increases. At $\theta = 67.5^\circ$, as shown in Fig. 10b, the maximum velocity ($V_m = 0.59$–0.67 m/s) is comparatively less than at $\theta = -27^\circ$ and occurs at $r = 2.49$ m. Velocity exceeds $½V_m$ over a width of 1.44 m = $2.36b_0$, and has a range of 0.16–0.63 m/s. Here the velocity increases radially away from the pool centre; reaching a maximum velocity in the outer portion of the pool. At $\theta = 112.5^\circ$, as shown in Fig. 10c, maximum velocity ($V_m = 0.57$–0.72 m/s) occurs at $r = 3.15$ m. Velocity ranges from 0 to 0.72 m/s, and increases radially away from the pool centre reaching a maximum velocity adjacent to the side wall. This distribution is followed until high velocity flow moves off the side wall and enters the downstream slot at $\theta = 200^\circ$. The centre baffle wall forces flow through the middle of the pool in Design 3 and forces flow to maintain a bell shaped distribution at $\theta = 67.5^\circ$, and $112.5^\circ$.

In all designs the pool's maximum turbulent kinetic energy is in the upstream slot, $K_m$, see Fig. 11. $K_m$ is lowest at 0.13$h$ and highest at 0.8$h$, increasing with elevation through the water column. In Design 1, $K_m$ is 0.072 $m^2/s^2$ at $z = 0.13h$, 0.108 $m^2/s^2$ at $z = 0.8h$, and 0.119 $m^2/s^2$ at $z = 0.8h$. The rate of increase is similar in the other designs. In the 7 designs tested $K_m$ ranged from 0.061 to 0.105 $m^2/s^2$ at $z = 0.13h$, 0.099 to 0.120 $m^2/s^2$ at $z = 0.5h$, and 0.110

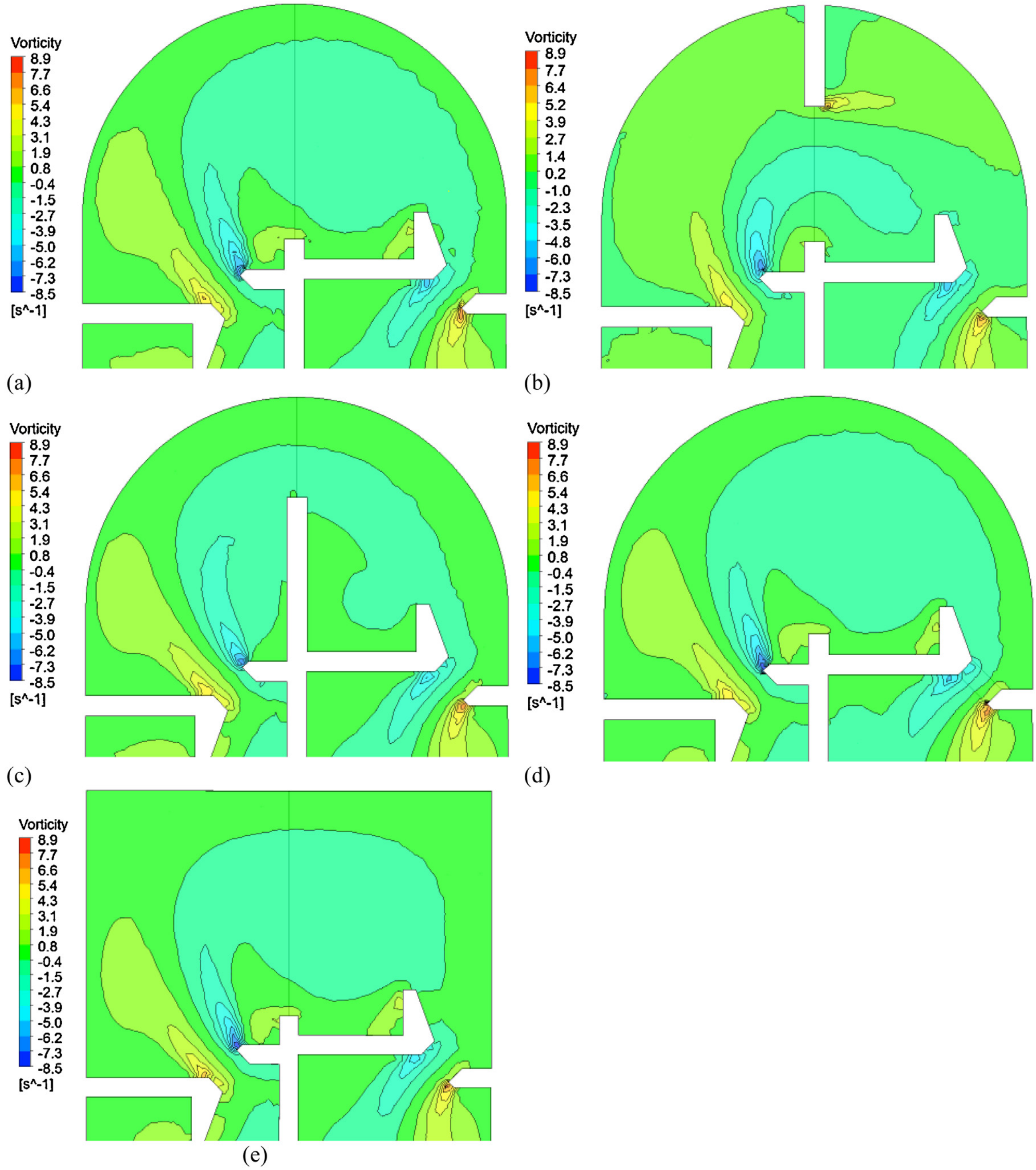


**Fig. 12.** Vorticity levels at depth $z = 0.5h$ in turning pool designs: (a) Design 1, (b) Design 3, (c) Design 4, (d) Design 6, and (e) Design 7.

to 0.128 $m^2/s^2$ at $z = 0.8h$. Despite the increase with elevation, the pattern is consistent in all designs through the water column. Turbulent kinetic energy levels are lower in the pool than at the slot. At $z = 0.5h$ the maximum turbulent kinetic energy in the pool ranged from 0.075 to 0.078 $m^2/s^2$. Maximum $K$ in the pool occurs along the upstream side wall at the beginning of the arcing back wall in Designs 1, 4, 6, and 7, and at the upstream edge of the vertical wall in Design 3. Throughout the remainder of the pool $K$ levels are lower. Through the full height of the water column levels are 'high' ($K > 0.05$ $m^2/s^2$) at $K_m$ and at the point of maximum $K$ in the pool, and 'low' ($K \leq 0.05$ $m^2/s^2$) in the rest of the pool. Typically, $K < 0.02$ $m^2/s^2$ in the downstream half of the pool.

For all designs vorticity in the horizontal plane, $\omega_z$, is highest adjacent to the entrance and exits slots, see Fig. 12. The maximum vorticity magnitudes ranged from 7.2 to 10.5 $s^{-1}$, and $\omega_z$ was uniform at the three depths evaluated. Areas where $\omega_z$ exceeds 5.0 $s^{-1}$ are very small. Throughout the pool $\omega_z$ is typically less than 3.0 $s^{-1}$.

## 4. Discussion and concluding remarks

Velocity and turbulence results for turning pools in this study were found to be comparable to regular pools in vertical slot fishways. For Designs 1, 4, 6, and 7 flow structure is a turbulent plane jet in the upstream section of the pool. The structure changes as flow moves into the middle of the pool, where velocity increases radially from the centre to the outside of the pool. This distribution is held until flow enters the downstream slot. The rate of maximum velocity ($V_m$) decay is linear for $x_m < 2.5$ m, then velocity is constant through $x_m \cong 2.5$–$9.0$ m, and then $V_m$ rapidly increases for

$x_m > 9.0$ m until reaching the downstream slot. Extending a baffle wall into the centre of the pool from the back wall, as per Design 3, deflects high velocity flow through the centre of the pool. As a result $V_m$ travels a shorter flow distance, with greater $V_m$ magnitudes as compared to other designs. Extending a baffle wall into the centre of the pool from the centre wall, reduces $V_m$ magnitudes through the pool. Consequently, $V_m$ magnitudes in Design 4 are lower than other designs.

The maximum slot velocity vector ($V_{sm}$) measured in the field and simulated in the 7 designs is within a passable range for adult lake sturgeon when adopting a prolonged swimming mode (Peake et al., 1997) and should not hinder upstream passage. Average volumetric energy dissipation ($\bar{\varepsilon}$) was calculated at $29\,\mathrm{W/m^3}$ in the turning pool. Volumetric energy dissipation is generally considered acceptable if $\bar{\varepsilon} < 200\ \ \mathrm{W/m^3}$ for salmonids, and if $\bar{\varepsilon} < 150\ \ \mathrm{W/m^3}$ for cyprinids (Larinier, 2008; Rodriguez et al., 2006). For American/Allis shad and weaker riverine species, Larinier (2002) suggested $\bar{\varepsilon}$ should be less than $150\,\mathrm{W/m^3}$. Kynard et al. (2011) observed successful passage of cultured lake sturgeon through a side-baffle spiral fishway when $\bar{\varepsilon}$ was $196\,\mathrm{W/m^3}$. As compared to an adjacent regular pool, the width of a turning pool in the site fishway is twice the size which reduces the average volumetric energy dissipation by half.

In all simulated designs the maximum turbulent kinetic energy ($K_m$) was in the upstream slot and increased with elevation through the water column. Maximum turbulent kinetic energy was typically only categorized as high ($K > 0.05\,\mathrm{m^2/s^2}$) in the vertical slots, and low ($K < 0.05\,\mathrm{m^2/s^2}$) throughout the remainder of the pool for all designs. Comparatively, maximum turbulence levels have been measured at $0.113\,\mathrm{m^2/s^2}$ in a regular pools (Liu et al., 2006), $0.0676\,\mathrm{m^2/s^2}$ in pool-type fishway (Silva et al., 2011), $0.4–1.2\,\mathrm{m^2/s^2}$ in a pool with orifice fishway (Guiny et al., 2005), and $0.6\,\mathrm{m^2/s^2}$ in a culvert retrofitted with baffles for fish passage (Morrison et al., 2008). The lower turbulence closer to the pool floor indicates that benthic species will typically incur a lower energetic cost during fishway ascension, although the threshold at which fishes are negatively affected by $K$ may vary between species. Maximum vorticity ranged from 7.2 to $10.5\,\mathrm{s^{-1}}$ and occurred adjacent to the entrance and exit slots. Further study is needed to identify the levels where individual species are affected by turbulent kinetic energy and vorticity.

Vortices with length and width dimensions greater than $l_f$ of the largest fish using the site's fishway (Thiem et al., 2011, 2013) were present in all designs, and could potentially disorient or destabilize fish (e.g., Tritico and Cotel, 2010; Webb and Cotel, 2010; Silva et al., 2012). The addition of a baffle wall to the centre of the pool in Designs 3 and 4 reduced the size of the vortex in the pool's centre by splitting it into smaller vortices. In both designs the downstream vortex has low velocities ($V \leq 0.2$ m/s) and is hydraulically suitable to act as a resting area for migrating fish, as recommended by some authors including for sturgeon fishway passage (e.g., Webber et al., 2007). The other designs tested do not have areas suitable to act as resting areas, and Design 4 is recommended over Design 3 due to the lower pool velocities observed. In Design 4 the ratio of centre baffle wall to length of turning pool is approximately 3:5. This ratio is recommended from this study, further investigation may be required to optimize this ratio. The addition of a baffle wall to Design 7, as per the dimensions and position of the baffle wall in Design 4, would make it a recommendable alternative to Design 4. This will reduce the size of the vortex in the pool's centre and provide a low velocity zone suitable for fish to rest. The straight back wall in Design 7 is less expensive to build than the semi-circular back wall in the other designs. Therefore, by adding a baffle wall to its centre Design 7 becomes a less expensive design alternative to Design 4 and is recommended for further study.

To further advance the science of fish passage design, particularly for turning pools in vertical slot fishways, it is necessary to construct and field test the hydraulics and fish passage performance of the recommended designs outlined in this paper. Anecdotally, a primary function of turning pools is to provide resting areas to fish (Rajaratnam et al., 1997). However, the research conducted here in terms of field hydraulic measurements, and CFD modelling as well as observations from field studies of sturgeon passage reveals that some turning pool designs fail to provide resting opportunities and may represent confusing and challenging hydraulic features. Additional research on the biological and hydraulic aspects of turning pools is needed to improve guidelines, inform future designs, and to potentially enable the modification of existing ones.

## Acknowledgements

We thank Chris Krath of the University of Alberta and Travis Raison of Carleton University for their invaluable field assistance during July 2011; Pierre Dumont and staff of Ministère des Ressources naturelles et de la Faune du Québec, and Parks Canada staff at Saint Ours for site access and logistical coordination of field work during July 2011. Thank you also goes out to Mat Langford of the University of Alberta and Simon Plourde formerly of Carleton University for their AutoCAD assistance. Funding for this project was provided by the NSERC HydroNET research network.

## References

ANSYS Incorporated, 2009. ANSYS CFX-Solver Theory Guide. ANSYS Inc., Canansburg, PA.

Baki, A.B.M., Zhu, D.Z., Rajaratnam, N., 2013. Mean flow characteristics in a rock-ramp type fishpass. J. Hydraul. Eng. 140 (2), 0000816, http://dx.doi.org/10.1061/(ASCE) HY. 1943-7900.

Brackbill, J., Kothe, D., Zemach, C., 1992. A continuum method for modeling surface tension. J. Comput. Phys. 100, 335–354.

Brown, M.E., Crandall, V., Flagg, L., 2010. Androscoggin river Anadromous fish restoration program. Final report. Department of Marine Resources Bureau of Sea Run Fisheries & Habitat, ME 04333-0021.

Bunt, C.M., 2001. Fishway entrance modifications enhance fish attraction. Fish. Manag. Ecol. 8, 95–105.

Bunt, C.M., Castro-Santos, T., Haro, A., 2012. Performance of fish passage structures at upstream barriers to migration. River Res. Appl. 28, 457–478.

Bunt, C.M., Cooke, S.J., McKinley, R.S., 2000. Assessment of the Dunnville fishway for passage of walleyes from Lake Erie to the Grand River, Ontario. J. Great Lakes Res. 26, 482–488.

Clay, C.H., 1995. Design of Fishways and Other Fish Facilities, 2nd ed. Lewis Publishers, Ann Arbor, MI.

Enders, E.C., Boisclair, D., Roy, A.G., 2003. The effect of turbulence on the cost of swimming for juvenile Atlantic salmon. Can. J. Fish. Aquat. Sci. 60, 1149–1160.

Enders, E.C., Boisclair, D., Roy, A.G., 2005. A model of total swimming costs in turbulent flow for juvenile Atlantic salmon (*Salmo salar*). Can. J. Fish. Aquat. Sci. 62, 1079–1089.

Fernandes, J., Lisboa, P., Simoes, P., Mota, J., Saatdjian, E., 2009. Application of CFD in the study of supercritical fluid extraction with structured packing: wet pressure drop calculations. J. Supercrit. Fluids 50 (1), 61–68.

Fernandes, J., Simoes, P., Mota, J., Saatdjian, E., 2008. Application of CFD in the study of supercritical fluid extraction with structured packing: dry pressure drop calculations. J. Supercrit. Fluids 47 (1), 17–24.

Guiny, E., Ervine, D., Armstrong, J., 2005. Hydraulic and biological aspects of fish passes for Atlantic salmon. J. Hydraul. Eng. 131 (7), 542–553.

Hatry, C., Binder, T.R., Thiem, J.D., Hasler, C.T., Smokorowski, K.E., Clarke, K.D., Katopodis, C., Cooke, S.J., 2013. The status of fishways in Canada: trends identified using the national CanFishPass database. Rev. Fish Biol. Fish. 23, 271–281.

Jamieson, E., Rennie, C., Townsend, R., 2013. Turbulence and vorticity in a laboratory channel bend at equilibrium clear-water scour with and without stream barbs (submerged groynes). J. Hydraul. Eng. 139 (3), 259–268.

Katopodis, C., Kells, J.A., Acharya, M., 2001. Nature-like and conventional fishways; alternative concepts? Can. Water Resour. J. 26, 211–232.

Katopodis, C., Williams, J.G., 2012. The development of fish passage research in a historical context. Ecol. Eng. 48, 8–18.

Khan, L.A., 2006. A three-dimensional computational fluid dynamics (CFD) model analysis of free surface hydrodynamics and fish passage energetics in a vertical-slot fishway. N. Am J. Fish. Manage. 26, 255–267.

Khan, L.A., Wicklein, E.A., Rashid, M., 2005. A 3D CFD model analysis of the hydraulics of an outfall structure at a power plant. J. Hydroinformatics 7 (4), 283–290.

Kirkgoz, M.S., Akoz, M.S., Oner, A.A., 2009. Numerical modeling of flow over a chute spillway. J. Hydraul. Res. 47 (6), 790–797.
Kynard, B., Pugh, D., Parker, T., 2011. Passage and behaviour of cultured lake sturgeon in a prototype side-baffle fish ladder: I. Ladder hydraulics and fish ascent. J. Appl. Ichthyol. 27 (Suppl. 2), 77–88.
Larinier, M., 2002. Chapter 5: Pool fishways, pre-barrages, and natural bypass channels. Bull. Fr. Peche Piscic. 364 (Suppl.), 54–82.
Larinier, M., 2008. Fish passage experience at small-scale hydro-electric power plants in France. Hydrobiologia 609, 97–108.
Launder, B., Spalding, D., 1974. The numerical computation of turbulent flows. Comput. Methods Appl. Mech. Eng. 3 (2), 269–289.
Liu, M., Rajaratnam, N., Zhu, D.Z., 2006. Mean flow and turbulence structure in vertical slot fishways. J. Hydraul. Eng. 132 (8), 765–777.
Lupandin, A.I., 2005. Effect of flow turbulence on swimming speed of fish. Biol. Bull. 32 (5), 461–466.
Ma, L., Ashorth, P.I., Best, J.L., Elliott, L., Ingham, D.B., Whitcombe, L.J., 2002. Computational fluid dynamics and the physical modelling of an upland urban river. Geomorphology 44, 375–391.
Marriner, B.A., MSc Thesis 2013. Hydraulics of the vertical slot fishway, a case study on the Vianney-Legendre fishway in Quebec, Canada. University of Alberta, Alberta, Canada.
Morrison, R., Hotchkiss, R., Stone, M., Thurman, D., Horner-Devine, A., 2008. Turbulence characteristics of flow in a spiral corrugated culvert fitted with baffles and implications for fish passage. Ecol. Eng. 35, 381–392.
Noonan, M.J., Grant, J.W.A., Jackson, C.D., 2012. A quantitative assessment of fish passage efficiency. Fish Fish. 13, 450–464.
Nortek AS, 2009. Vectrino Velocimeter User Guide. Nortek AS, Vangkroken, Norway.
Pavlov, D.S., Lupandin, A.I., Skorobogatov, M.A., 2000. The effects of flow turbulence on the behaviour and distribution of fish. J. Ichthyol. 40 (2), S232–S261.
Peake, S., Beamish, F.W.H., McKinley, R.S., Scruton, D.A., Katopodis, C., 1997. Relating swimming performance of lake sturgeon, *Acipenser fulvescens*, to fishway design. Can. J Fish. Aquat. Sci. 54, 1361–1366.
Pon, L.B., Hinch, S.G., Cooke, S.J., Patterson, D.A., Farrell, A.P., 2009. Physiological, energetic and behavioural correlates of successful fishway passage of adult sockeye salmon *Oncorhynchus nerka* in the Seton River, British Columbia. J. Fish Biol. 74, 1323–1336.
Puertas, J., Pena, L., Teijeiro, T., 2004. Experimental approach to the hydraulics of vertical slot fishways. ASCE J. Hydraul. Eng. 130, 10–23.
Rajaratnam, N., 1976. Turbulent Jets. Elsevier Scientific, Amsterdam, The Netherlands.
Rajaratnam, N., Katopodis, C., Solanki, S., 1992. New designs for vertical slot fishways. Can. J Civ. Eng. 19, 402–414.
Rajaratnam, N., Katopodis, C., Wu, S., Saburm, M.A., 1997. Hydraulics of resting pools for Denil fishways. ASCE J. Hydraul. Eng. 123 (7), 632–638.
Rodriguez, T.T., Agydo, J.P., Mosquera, L.P., 2006. Evaluating vertical-slot fishway designs in terms of swimming capabilities. Ecol. Eng. 27, 37–48.
Roscoe, D.W., Hinch, S.G., 2010. Effectiveness monitoring of fish passage facilities: historical trends, geographic patterns and future directions. Fish Fish. 11, 12–33.
Schlumberger Water Services, 2011. Mini-Diver Product Manual. Schlumberger Water Services, Delft, The Netherlands.
Silva, A., Katopodis, C., Santos, J., Ferreira, M., Pinheiro, A., 2012. Cyprinid swimming behaviour in response to turbulent flow. Ecol. Eng. 44, 314–328.
Silva, A.T., Santos, J.M., Ferreira, M.T., Pinheiro, A.N., Katopodis, C., 2011. Effects of water velocity and turbulence on the behaviour of Iberian barbell (*Luciobarbus bocagei*, Steindachner 1864) in an experimental pool-type fishway. River Res. Appl. 27, 360–373.
Thiem, J., Binder, T., Dawson, J., Dumont, P., Hatin, D., Katopodis, C., Zhu, D.Z., Cooke, S., 2011. Behaviour and passage success of upriver-migrating lake sturgeon *Acipenser fulvenscens* in a vertical slot fishway on the Richelieu River, Quebec, Canada. Endang. Species Res. 15, 1–11.
Thiem, J.D., Binder, T.R., Dumont, P., Hatin, D., Hatry, C., Katopodis, C., Stamplecoskie, K.M., Cooke, S.J., 2013. Multispecies fish passage behaviour in a vertical slot fishway on the Richelieu River, Quebec Canada. River Res. Appl. 29, 582–592.
Tritico, H.M., Cotel, A.J., 2010. The effects of turbulent eddies on the stability and critical swimming speed of creek chub (*Semotilus Atromaculatus*). J. Exp. Biol. 213, 2284–2293.
Webb, P.W., Cotel, A.J., 2010. Turbulence: does vorticity affect the structure and shape of body and fin propulsors? Integr. Comp. Biol. 50 (6), 1155–1166.
Webber, J.D., Chun, S.N., Maccoll, T.R., Mirise, L.T., Kawabata, A., Anderson, E.K., Sung Cheong, T., Kavvas, L., Mcgee Rotondo, M., Hochgraf, K.L., Churchwell, R., Cech Jr., J.J., 2007. Upstream swimming performance of adult white sturgeon: effects of partial baffles and a ramp. Trans. Am. Fish. Soc. 136, 402–408.
White, L.J., Harris, J.H., Keller, R.J., 2011. Movement of three non-salmonid fish species through a low-gradient vertical slot-fishway. River Res. Appl. 27, 499–510.
Williams, J.G., Armstrong, G., Katopodis, C., Larinier, M., Travade, F., 2012. Thinking like a fish: a key ingredient for development of effective fish passage facilities at river obstructions. River Res. Appl. 28, 407–417.
Wu, S., Rajaratnam, N., Katopodis, C., 1999. Structure of flow in vertical slot fishway. J. Hydraul. Eng. 125 (4), 351–360.